Fabrication of engineered M13 bacteriophages into liquid crystalline films and fibers for directional growth and encapsulation of fibroblasts†

Woo-Jae Chung, Anna Merzlyak and Seung-Wuk Lee*

Received 3rd April 2010, Accepted 30th June 2010
DOI: 10.1039/c0sm00199f

We report on a novel method to utilize genetically engineered M13 phages as functional nano building blocks that can form structurally aligned film and fiber matrices for tissue engineering scaffolds. Two- and three-dimensional directionally aligned long range ordered structures were constructed using shearing and polyionic complexation with cationic polymers. Further we have demonstrated that aligned phage-based tissue engineering materials can guide and stimulate the growth of the target fibroblasts. Our phage-based tissue engineering scaffolds can be used for providing micro and macroscopic control of cell behaviors.

Introduction

Designing biomimetic matrices to control biochemical, physical and mechanical cues to regulate cell behavior is one of the critical issues for the development of tissue regenerating materials.[1–5] The requisite design considerations for tissue engineering materials are based on the cellular environment *in vivo*, where cells are in close contact with other cells as well as with the extracellular matrix (ECM). ECM consists of an interconnected network of nanofibrous proteins and proteoglycans, which form self-organized structures to provide topographical cues and physical support of various stiffness for cell polarization or migration.[6–8] Furthermore, ECM provides chemical signals to guide and control cells' fates and functions.

Numerous natural and synthetic polymers are being explored to engineer tissue scaffolds that can closer approximate the native ECM. The most common approach is to fabricate these matrices from synthetic, biodegradable (or resorbable) materials such as poly(L-lactic acid) and poly(glycolic acid)[9,10] or from natural materials such as collagen, fibrin, and alginate.[11–14] These scaffolds are seeded with the desired cells, which proliferate or differentiate to form organized cellular structures. Recently, various nanomaterials and nanotechnologies have been developed for the bottom-up assembly of three-dimensional *in vivo*-mimetic cellular environments. Fibrous network scaffolds have been prepared using electro-spinning,[8,9] peptide self-assembly[15–17] and polymer phase separation.[2,18] The controlled display of cell-signaling peptides or proteins in these structures have shown many promising results *in vivo*, demonstrating that such structures may be used in the future for regenerative medicine.[12] More recently, engineered viruses, including M13 bacteriophage (phage) and tobacco mosaic viruses (TMV) have gained attention as potential tissue engineering materials.[19–22] Advantages that have been demonstrated in the use of such building blocks are their abilities to self-assemble into directionally organized structures,[19,23,24] and to present functional motifs with well-defined spacing either through genetic engineering or chemical conjugation.[19–21,25] In particular, our group has demonstrated the potential use of genetically engineered phages as tissue regenerating scaffolds for guiding neural cell behavior.[20] Previously, liquid crystalline suspensions of genetically engineered phages and neuronal progenitor cells (NPCs) were extruded into liquid agarose, which, after gelling, entrapped the assembled phages and cells. The engineered phage-based matrices possessed nematic phase alignment with their director parallel to the long axis of the fiber, and supported the differentiation and extension of neurites in a direction parallel to the long axis of the fiber. However, the fibrous scaffold was confined in the agarose gel, restricting the flexibility of further engineering parameters as compared to self-standing fibers. Here, we present a facile approach to exploit genetically engineered M13 phages to construct directionally organized two and three-dimensional scaffold structures that can control chemical and physical cues for fibroblast cell growth as well as encapsulation (Fig. 1). Because the phage coat proteins are negatively charged, positively charged substrates or cationic polymers were utilized to stabilize the self-assembled phage structures by providing better adhesion or by interfacial electrostatic assembly of cationic polymer/phage complexes. NIH-3T3 fibroblasts were shown to responded to chemical and physical cues from the directionally organized phage-based scaffolds and were successfully grown within the three dimensional microfiber matrices. Our approach may be useful for construction of novel tissue regenerating materials as well as for cell-based drug delivery.

Materials and methods

Genetic engineering of M13 bacteriophage

M13 bacteriophage were engineered to display specific peptide motifs on their major coat proteins (pVIII) by using a partial library cloning approach.[20] An octapeptide was inserted at the N-terminus of the pVIII and positioned between the first and the fifth amino acids of the wildtype pVIII, replacing residues 2–4 (Ala-**Glu-Gly-Asp**-Asp to Ala-(**Insert**)-Asp). To facilitate recircularization of the engineered plasmid, a Pst I restriction site was created by mutating the nucleic acid base at position 1372 of

1-220 Donner Lab, Bioengineering, University of California, Berkeley, CA, 94720, USA. E-mail: leesw@berkeley.edu; Fax: +1-510-486-6488; Tel: +1-510-486-4628

† Electronic supplementary information (ESI) available: Experimental procedure and additional supporting figures are provided. See DOI: 10.1039/c0sm00199f

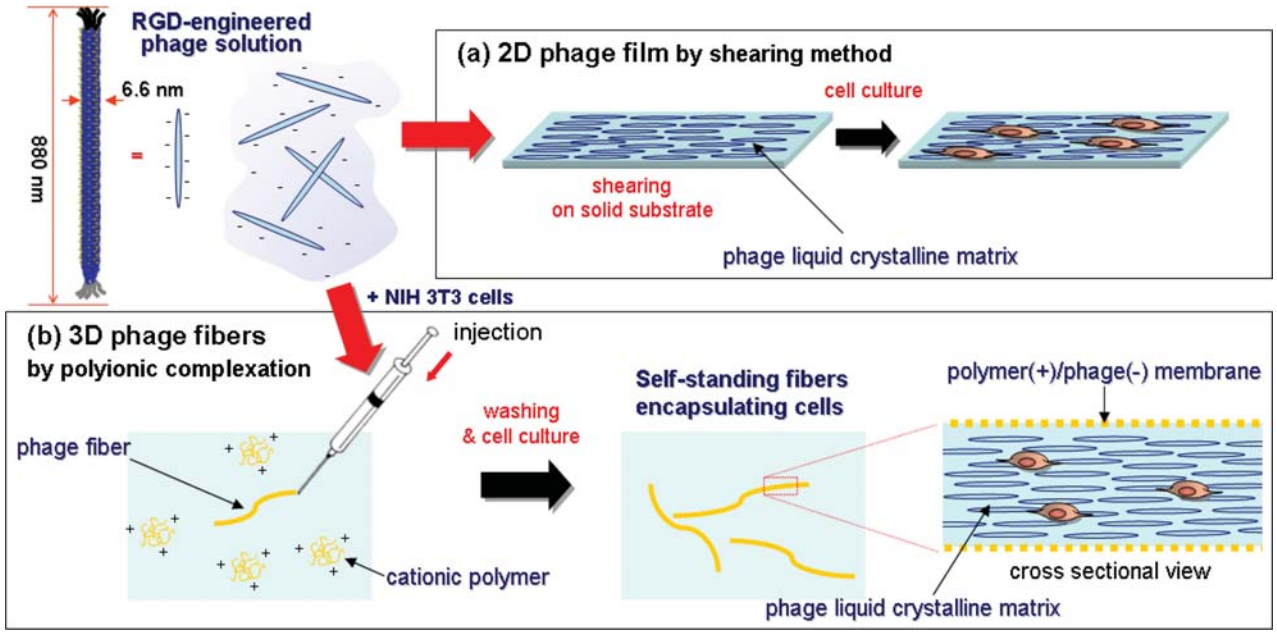

Fig. 1 Schematic illustration representing assembly of genetically engineered phages into phage-based films and fibers. (a) Two-dimensional liquid crystalline phage films were constructed by shearing M13 phage solutions on substrates to align phages for directing cell growth. (b) Liquid crystalline suspensions of negatively charged engineered M13 phage are injected into positively charged polymer aqueous solutions to form aligned phage fibers based on interfacial polyionic complexation. Cells were co-injected with M13 phage solutions for cell encapsulation.

M13KE vector (NEBiolabs, Ipswich, MA) from T to A using a QuikChange® Kit (Stratagene, La Jolla, CA). Two primers were designed to insert the desired peptide: 5′ATATATCTGCAGNN(NNN)$_2$*CGTGGTGAC*(NNN)$_2$GA-TCCCGCAAAAGCGGCCTTTAATCCC3′, for RGD-phage, and 5′GCTGTCTTTCGCTGC-AGAGGGTG3′, to linearize the vector (insert underlined, RGD shown in italics, N = A, T, G or C). To incorporate the gene sequences, polymerase chain reaction (PCR) was performed using Phusion™ High-Fidelity DNA Polymerase (Finnzymes, Espoo, Finland). The obtained product was purified and transformed into XL1-Blue electroporation competent bacteria (Stratagene, La Jolla, CA). RGE-phage was engineered *via* the same cloning method to serve as a sequence specific control for the RGD-phage. The primer was designed to match the RGD-phage exactly but with glutamic acid substituted to aspartic acid. Forward primer to construct the RGE-phage was 5′ATATATCTGCAGACTCGGGACGTG-GTGAAACCGAAGATCCCGCAAAAG-CGGCCTTTAAC-TCCC3′, with a resulting sequence ADSG*RGE*TEDP. The constructed phages were amplified using bacterial cultures and purified through the standard polyethylene glycol precipitation method.[26] The phage solution was further purified by filtration through 0.45 μm pore size membranes. To verify phage stability, DNA sequences were confirmed at each step of the amplification.

Phage film fabrication

Glass slide substrates were placed in piranha solution for 10 min (H_2O_2:H_2SO_4 = 1 : 4), thoroughly rinsed with DI water and dried under a nitrogen stream. Then, the substrates were treated with 1% (v/v) 3-aminopropyl triethoxysilane (APTS) solution in EtOH. Subsequently, the substrates were rinsed with EtOH to remove excess silane and annealed at 100 °C for 10 min. For preparation of phage films (randomly oriented topography), phage solutions (50 μL of 10^{12} viruses/mL) in PBS were spread on the APTS-treated glass surface (1 × 1 cm^2) and allowed to dry overnight at 37 °C in a humidified incubator. For preparation of aligned phage films with directionally aligned topography, a droplet (5 μL) of the phage solution (10–30 mg/mL) was placed on one edge of the APTS-treated glass substrate (0.5 × 1.5 cm^2) and dragged using a glass slide parallel to the long axis of the glass substrate. The film samples were dried overnight at room temperature and rinsed with PBS prior to cell culture experiments.

NIH-3T3 fibroblasts culture on phage films

NIH-3T3 fibroblasts (University of California, Berkeley Cell Facility) at passage number 20–28 were seeded on phage films and laminin-coated substrates and cultured in serum-free media (DMEM/F12 1 : 1) (Gibco Life Science, Grand Island, NY) at 37 °C with 5% CO_2 for different times. Viability was assessed with the Live/Dead® Viability test (Invitrogen, Carlsbad, CA) according to the manufacturer's instruction. Briefly, the cells were rinsed with PBS and then incubated with 2 μM calcein acetomethoxy (AM) and 4μM ethidium homodimer-1 solutions for 20 min at 37 °C. Then, the cells were rinsed again, and observed by a fluorescent microscope. The number of live and dead cells was counted with the particle analysis function of ImageJ software (NIH, http://rsb.info.nih.gov/ij/), from 5 separate fields of view. We quantified the viability of NIH-3T3 fibroblast cells on the genetically engineered phage film by observing their growth on these substrates for the duration of five days.

Fluorescence microscopy imaging of cells cultured on phage film

Cells cultured on the phage films were fixed in 4% paraformaldehyde for 30 min and then blocked with a solution of 0.3% Triton X-100 and 5% normal goat serum in PBS for 30 min. To visualize the NIH-3T3 fibroblasts, actin filaments were stained with Alexa Fluor 488 phalloidin (Molecular Probes, Eugene, Oregon), at a dilution of 1 : 50 in PBS, for 2 h at room temperature. The cells were then rinsed with PBS, and the nuclei counterstained with DAPI (300 nM). To confirm whether the surface is covered with phage particles, the phage film samples were incubated with the rabbit anti-fd antibody (1 : 500, Sigma Aldrich, St. Louis, MO) for 2 h at room temperature and after rinsing with PBS, secondary goat Alexa Fluor 546 conjugated antibodies (Molecular Probes, Eugene, OR) were used at a dilution of 1 : 250 for 2 h at room temperature. The fluorescence images were collected using an IX71 fluorescence microscope (Olympus, Tokyo, Japan).

Cell encapsulation in phage-based fibers by polyionic complex formation at the interface

Liquid crystalline suspension (1–20 mg/ml) of engineered phage was prepared and diluted with PBS. This suspension was then manually injected at a rate of approximately 0.8 ± 0.1 μL/s, directly into the cationic polymer solution in PBS (0.2% w/v). The cationic polymers include poly(ethylene imine) (PEI, Mw ~60 kDa), chitosan (Mw ~150 kDa), and poly-L-lysine (PLL, Mw 15–30 kDa) (Sigma Aldrich, St. Louis, MO). After one minute, the resulting fibers were washed with PBS (10 times). To block positive charges at the outer surface, the fibers were treated with alginate in PBS solution (0.5% w/v) for 1 min and then washed with PBS (10 times). For cell encapsulation, NIH-3T3 fibroblast cells in culture media (1–2 × 10^6 cells/mL) were added to the phage solution (15 mg/mL) in 1 : 5 (v/v) mixture (final phage concentration: 12.5 mg/mL). Subsequently, the cell mixture solution was injected into cationic polymer solution and washed as above. Finally, the cell-encapsulating fibers were placed in the cell culture media (DMEM supplemented 10% FBS) and incubated at 37 °C, 5% CO_2 and 95% humidity. The culture media was changed every three days. The viability of encapsulated cells was tested after 3, 5, 7 and 10 days, using Live/Dead® Viability test (Invitrogen, Carlsbad, CA). Calcein-AM (1 μM) and ethidium homodimer-1 (5 μM) in PBS solution was added to the cell-encapsulating fibers. The images were collected with a Zeiss 510 UV/VIS Meta laser scanning confocal microscope. The number of live and dead cells was counted with spot analysis tool of the Imaris software (Bitplane Inc., Saint Paul, MN). Survival rates of cells cultured in three-dimensional phage fibers were analyzed. At the later time points of the analysis the percentage of viable cells was slightly underestimated, due to the large dense clusters of cell colonies, which made it difficult for the software to account for all of the cells individually.

Results and discussion

Cell viability and chemical cue effects of the engineered phages on fibroblast cell growth

We cultured NIH-3T3 fibroblasts on the drop-cast phage films to evaluate the specificity of cell response to the RGD-, RGE- and wildtype-phage, as compared to the behavior of the cells grown on control laminin-coated substrates. Soluble growth factors and cell adhesive proteins such as fibronectin and vitronectin in the serum (e.g. FBS) are known to exert an effect on non-specific cell adhesion and growth.[27] Therefore, in order to exclude the effect of integrin binding proteins contained in FBS, or secreted by the cells, the cells were cultured in serum-free media (DMEM/F12 1 : 1) and observed at earlier times 1.5–6 h (supplementary information Fig. S1). When grown in serum-free media for 4 h, fibroblasts on RGD-phage film showed a more elongated cell morphology as compared to cells on RGE- and wildtype-phage films, and had a similar spreading behavior to the cells cultured on laminin coated substrates (Fig. 2a). Furthermore the quantity of attached cells was greater (~2 times) on the RGD-phage film as compared to other control-phage films, indicating a specific preference for cell attachment (Fig. 2b). To confirm if the cell adhesion was specific to RGD-phage recognition on the film, we conducted inhibition assays utilizing soluble RGD-phages. When the cells were seeded in the presence of soluble RGD-phages, the adhesion of fibroblasts on the RGD-phage film was strongly retarded and no spreading of cells was observed until 3 h after seeding (supplementary information Fig. S2). This inhibition assay revealed the specificity of the NIH-3T3 cell interaction

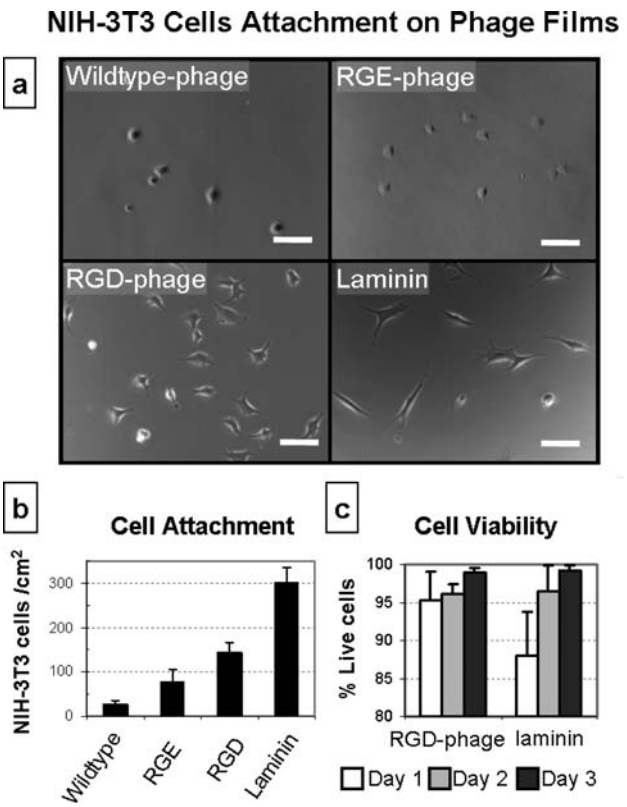

Fig. 2 Chemical cue effects of engineered phages on NIH-3T3 cells and their growth patterns. (a) Phase contrast images of NIH-3T3 fibroblasts cultured (4 h) on wildtype-, RGE-, RGD-phage and laminin coated substrates in serum-free culture media. (b) Counting of adhered NIH-3T3 cells on phage coated substrates after 2 h culture in serum-free media. (c) Cell viability on RGD-phage film and tissue culture plate. All experiments were performed by seeding 2 × 10^3 cells/cm^2 on the phage-coated substrates and laminin-coated substrate.

with RGD-phages. In addition, we tested cell viability on the RGD-phage dropcast film for 5 days. The survival rate of NIH-3T3 fibroblasts was over 85% on both RGD-phage films and normal tissue culture plates at all the time points tested (Fig. 2c), demonstrating that the phage-based film can support and sustain cell viability.

Physical cue effects of engineered phage on fibloblast cell growth

To explore the physical cues of engineered films on fibroblast cell growth, we constructed directionally ordered two-dimensional phage films. These films were prepared by using shear meniscus force methods as described in the Methods section. Atomic force microscope (AFM) images showed the apparent difference between the surface topology of phage films produced by drop-casting and by shearing the phage solution (Fig. 3a, b). The drop-cast phage film exhibited randomly oriented surface topography (Fig. 3a). On the other hand, the sheared phage film had a corrugated surface morphology with periodic, strongly directional grooves and ridges aligned parallel to the shear direction (Fig. 3b). The genetically engineered phage particles assembled together to form sub-micron fiber bundles with directionally aligned topography. The amplitude and topography roughness were tunable by applying different concentrations of phage solution (supplementary information, Fig. S3). There has been a wide range of reports on how size of the topographical features affects the behavior of different cell types.[7,28] Contact guidance depends on the cell's lack of ability to spread across an obstacle such as a sharp angle, ridge or a step, making it more favorable for the cell to make adhesions and therefore elongate and polarize on a more planar substrate.[6] The aligned phage fiber bundles with sub-micron diameter are expected to limit cell spreading across the phage film, and instead encourage the clustering of cell integrins and polarization of cells parallel to the long axis of the fibers. Cell alignment was determined by the angle between the longest axis of the cell body with respect to the shear direction. The elongation describing the extent to which the hypothetical ellipse is lengthened was calculated as the average ratio of the lengths of the long axis to the short axis of each cell. The cells cultured on RGD-phage aligned films began to extend their filamentous cytoskeleton in the direction of the shear within 2 h, whereas the cells on RGE- and wildtype-phage film were shown to remain more rounded (supplementary information Fig. S4), indicating the biochemical specificity of aligned RGD-phage films. To assess the cellular growth on each phage film, we measured elongation and orientation of cells (cultured for 12 h) using ImageJ. At 12 h after cell seeding the cells cultured on aligned RGD-phage film were seen to have the most elongated extension (elongation: 5.2 ± 2.9 ($n = 250$)). On the control phage film (RGE and wildtype), due to the lack of adhesive motifs on the film a much lower population of cells were seen on the surface (supplementary information Fig. S5). Even attached cells had substantially smaller elongation (RGE: 1.9 ± 1.1 ($n = 50$), wildtype: 2.0 ± 1.0 ($n = 50$)).

The orientation of the cell elongation was observed to be highly dependant on the anisotropic topography of the phage films. On RGD-phage film ~77% of the cells were aligned parallel to the shear direction within $\pm 10^\circ$ (Fig. 3c, e). On the control-phage films (RGE- and wildtype-) the orientational cell growth was less efficient (45–51% of cells within $\pm 10^\circ$) due to the poor cell elongation (Fig. 3e). Cells cultured on laminin-coated substrate were polygonal in shape and spread out in a radial fashion displaying no particular orientation (Fig. 3d, e).

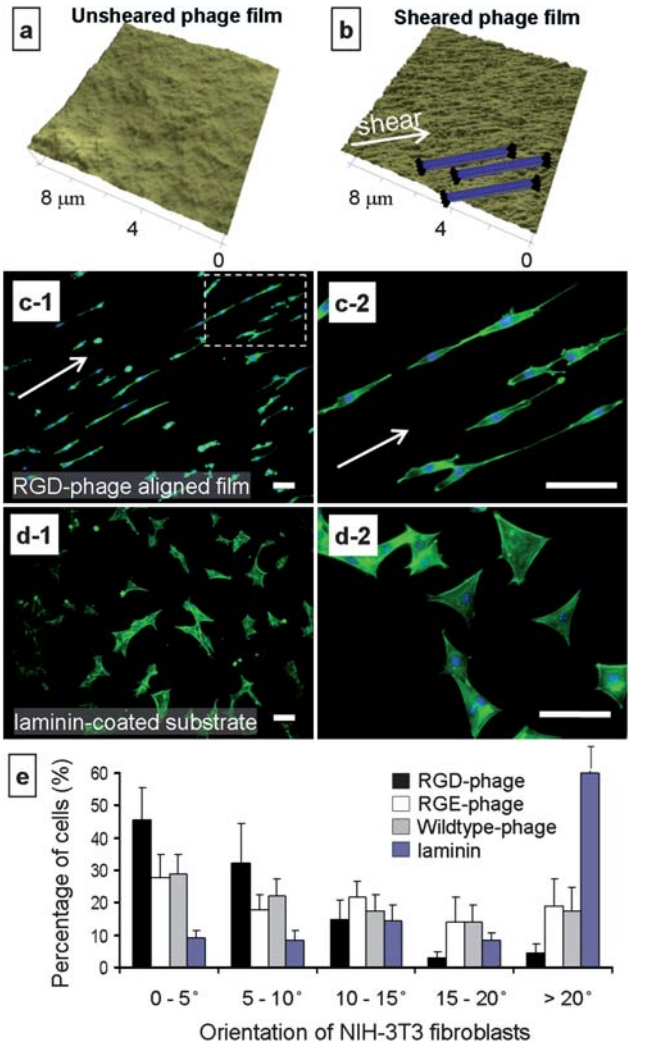

Fig. 3 Physical cue effects of RGD-engineered phage films on directional growth of NIH-3T3 fibroblasts. (a) AFM image of the RGD-phage film with randomly oriented topography prepared by drop-casting (30 μg/mL). (b) AFM image of the directionally aligned surface of the RGD-phage film prepared by meniscus shearing methods (20 mg/mL). Schematic inset diagram depicts the orientation of phage (Phages are not in scale). (c, d) Fluorescence images of fibroblasts grown on (c-1 and c-2) the RGD-phage aligned substrate and (d-1 and d-2) laminin-coated substrate in serum-free media after 12 h. Actin filaments stained with phalloidin (green), and nuclei counterstained with DAPI (blue). (e) Distribution of NIH-3T3 fibroblast orientation grown on the phage aligned films and laminin-coated substrate in serum-free media (after 12 h). The average orientation angle was taken from ten different areas (50–250 cells) on the film using ImageJ. All experiments were performed by seeding 3×10^4 cells/cm^2 on the phage films and laminin-coated substrate. All scale bars indicate 100 μm.

From the results, it was apparent that the behavior of the cells was influenced by the physical topography of the phage film. Our results show that the combined effects of biochemical (RGD motif) and physical cues of the phage material play a synergistic role in NIH-3T3 cell attachment, spreading and alignment.

Structures of phage-based fibers

Phage-based micro- and nano-fibers have previously been fabricated by spinning engineered M13 phages.[29,30] The resulting phage-based fibers were decorated with organic or inorganic materials, in which phage building blocks provided flexibility in design and engineering of the fiber surfaces for a variety of applications.[30] However, in order to extend the scope of biological application of phage-based fibers to encapsulate biomolecules and to support three dimensional cellular growth, novel microfiber fabrication strategies need to be developed. To exploit both the structure and functionality of the phage-based fibers and encapsulate biomolecules for 3D culture of cells, we developed novel phage-based fibers by simple microsyringe injection of the phage suspension (> 10 mg/mL) into poly-L-lysine (PLL) aqueous solutions as depicted in Fig. 1b. The resulting phage microfibers were 200–400 μm in diameter depending on the orifice diameter of the syringe needle and showed no limitation on their lengths (Fig. 4a). In this study, we mainly used a 23 gauge needle (~340 μm inner diameter) to create 280–400 μm fibers. Under polarized optical microscope the phage fibers prepared in such manner exhibited a uniform response along the long axis of the fiber, indicating that the phage fiber possesses nematic behavior, with director alignment parallel to the long axis of the fiber (Fig. 4b). The distribution of phage within the fiber was assessed by confocal fluorescence microscopy using FITC conjugated RGD-phage in the assembly process (Fig. 4c, d). Phage fibers prepared with lower phage concentrations 1–5 mg/mL exhibited a density gradient of phages perpendicular to the long axis of the fiber (Fig. 4c). The density of phages was higher at the outer surface due to the interaction with cationic polymers at the PLL/phage interface. When 10–15 mg/mL of phage solution was assembled into fibers, the distribution of phage throughout the fiber was relatively homogeneous implying that the liquid crystalline structure from the concentrated phage solution was preserved within the fiber (Fig. 4c). Under these conditions, PLL was mainly located at the outer surface constituting the contour of the fiber (Fig. 4d). The overall core-shell structure proved that the self-assembly based on electrostatic interaction occurred at the interface between two aqueous solutions and the resulting polyion complex membrane (PLL/RGD-phage) behaved as a diffusion barrier.

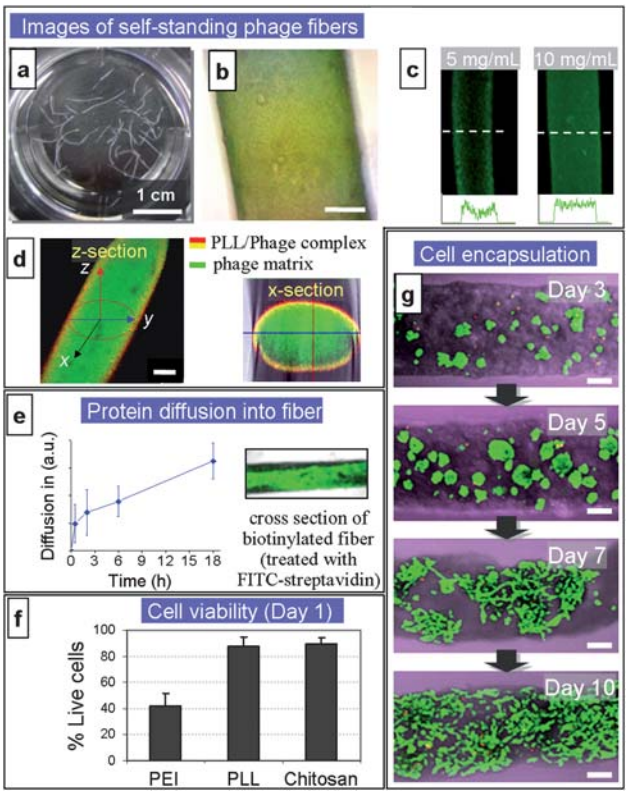

Fig. 4 3D Phage microfibers and their chemical and physical cue effects on fibrobasts. (a) Photograph of phage fibers and (b) POM image of a phage fiber prepared by extruding RGD-phage solution (1 μL of 12.5 mg/mL in PBS) into PLL solution (0.2% w/v in PBS). (c) Distribution of phages within the fiber matrix prepared by extruding different concentrations of RGD-phage solution (5 and 10 mg/mL) into RITC-conjugated PLL solution (0.2% w/v in PBS). (d) Core-shell structure of the phage fiber displaying outer polyionic complex layer and inner phage matrix. (e) FITC-streptavidin diffusion into biotinylated fiber. Biotinylated RGD-phage fibers (prepared from 12.5 mg/mL of phage solution) were treated with FITC-streptavidin (0.1 mg/mL in PBS) solution and the concentration of solution was measured at designated time. (f) Cell viability in the phage fibers with different polymer shell layers (PEI, PLL and chitosan) after day 1. (g) Confocal fluorescence images of encapsulated cells in the phage fiber (PLL/RGD-phage) grown for the period of time up to 10 days in DMEM media supplemented with FBS (10%) (Green: live cells, red: dead cells). For cell viability assay, the RGD-phage solution (15 mg/mL) was mixed with cell suspension in 5 : 1 (v/v) ratio (final phage concentration: 12.5 mg/mL). All scale bars indicate 100 μm.

Permeability of phage-fibers

For the purpose of cell encapsulation, encapsulating materials are required to have an outer membrane permeable to nutrients for supporting cell viability within the matrices.[31,32] To evaluate the feasibility of utilizing PLL/RGD-phage fibers as cell encapsulation materials, we investigated the permeability of PLL/RGD-phage fibers to a model protein, streptavidin. Biotinylated fibers were prepared from the assembly of biotinylated RGD-phages (*b*-RGD-phages) and PLL in the same way as described earlier. The use of FITC conjugated streptavidin allowed us to observe and quantify the diffusion of proteins into the *b*-RGD-phage fiber over time using fluorescence microscopy and UV/VIS spectrophotometer (Fig. 4e). Confocal z-section images showed that the proteins were able to diffuse across the membrane and reach the center of the phage fiber matrix (Fig. 4e (inset) and supplementary information Fig. S6). The amount of protein adsorption increased with time as the inward diffusion and specific binding between biotin and streptavidin underwent in the fiber, reflecting the promising aspects that our phage fibers are permeable to biomolecules and can support cell growth as a cell encapsulating material.

Fibroblast cell viability and growth in 3D phage-based fibers

Cationic polymers, including PLL, poly(ethylene imine) (PEI), and chitosan, were tested for NIH 3T3 fibroblast encapsulation, based on the polyionic complex formation at the interface with RGD-phage solutions (12.5 mg/mL). Cell viability was examined

with confocal microscopy imaging by live/dead assays for each of the cationic polymers tested after 1 day of incubation. PEI resulted in ~50% of cell survival whereas cell encapsulation using PLL and chitosan showed over 90% cell survival rates (Fig. 4f). Consequently, PLL and chitosan were chosen as the membrane forming polymers for their compatibility with cells in the encapsulation process. The cells were observed over a 10 day period after encapsulation using PLL and RGD-phage solution. Cells encapsulated in the phage fiber retained good viability (Fig. 4g). The cells proliferated over time in the three-dimensional fibers, reflecting that the phage fiber supports metabolic activity of viable cells. Live/dead assays of the encapsulated cells showed 85% survival rate throughout the experiment. The fibroblast cells within the fiber formed distributed colonies, which grew in size during the initial five days of culture. In contrast to the cell morphology on 2D phage films, the encapsulated cells were spherical in shape and didn't respond to the alignment of the phage nanofibers in the matrix within five days (Fig. 4g Day 3 & 5) Previously, we've demonstrated neurite extension of NPCs parallel in direction to the long axis of phage fibers entrapped in agarose.[20] The difference in cell morphologies on 2D and 3D matrices and between cell types may result from the differences in the matrix stiffness. Various cell types respond to material stiffness differently. For example, in general, a higher matrix stiffness (~3000Pa)[33,34] is required for fibroblasts to elongate on scaffold materials. Our three-dimensional liquid crystalline phage matrix with the polyionic complex membrane was not immediately stiff enough to support fibroblast cell spreading within the matrix as compared to the two dimensional phage film substrates which were supported with a hard substrate (glass). However, from day seven the cell cluster dissociation took place and the cells began to migrate along the inner matrix of the phage fiber (Fig. 4g Day 7 and 10). We believe this phenomenon was caused by an alteration of the phage matrix stiffness resulting from a continuous secretion and accumulation of extracellular components (proteins, proteoglycan, *etc.*) by the encapsulated cells in the fiber. The phage fiber was proven to support the cell viability and allow for an environment that could be remodeled by the encapsulated fibroblast cells to create optimal spreading and growth conditions, thus demonstrating its potential use as a material for tissue regeneration.

Conclusion

In conclusion, we report the novel architectural design of the phage-based tissue engineering scaffolds. We constructed long-range ordered two-dimensional liquid crystalline films and three dimensional fibers using facile meniscus shearing methods and solution extrusion methods respectively. The resulting phage-based 2D and 3D matrices exhibited good cytocompatibility and displayed controllable chemical and physical cues to guide cellular growth patterns of fibroblasts. In addition, 3D phage fibers and their phage/polymer complex membrane structures showed good permeability for various biomolecules and demonstrated the encapsulating capabilities of the phage-based scaffold materials. We anticipate that our versatile viral tissue engineering materials will provide new and inexpensive pathways to organize tissue scaffolds and to regulate cellular behaviors.

Acknowledgements

This work was supported by the Hellman Family Faculty Fund (SWL), start-up funds from the Nanoscience and Nanotechnology Institute at the University of California, Berkeley (SWL), the Korean Research Foundation Grant funded by the Korean Government (MOEHRD) (KRF-2006-352-D00048), and the Graduate Student Fellowship from the National Science Foundation (AM). We thank Eddie Wang for help in editing the manuscript.

Notes and references

1 R. Langer and J. P. Vacanti, *Science*, 1993, **260**, 920–926.
2 P. X. Ma, *Adv. Drug Delivery Rev.*, 2008, **60**, 184–198.
3 J. Patterson, M. M. Martino and J. A. Hubbell, *Mater. Today*, 13, pp. 14–22.
4 B. Murtuza, J. W. Nichol and A. Khademhosseini, *Tissue Eng., Part B: Rev.*, 2009, **15**, 443–454.
5 C. T. S. Wong Po Foo, J. S. Lee, W. Mulyasasmita, A. Parisi-Amon and S. C. Heilshorn, *Proc. Natl. Acad. Sci. U. S. A.*, 2009, **106**, 22067–22072.
6 A. S. Crouch, D. Miller, K. J. Luebke and W. Hu, *Biomaterials*, 2009, **30**, 1560–1567.
7 M. J. Dalby, M. O. Riehle, H. Johnstone, S. Affrossman and A. S. G. Curtis, *Cell Biol. Int.*, 2004, **28**, 229–236.
8 Z. Ma, M. Kotaki, R. Inai and S. Ramakrishna, *Tissue Eng.*, 2005, **11**, 101–109.
9 F. Yang, R. Murugan, S. Wang and S. Ramakrishna, *Biomaterials*, 2005, **26**, 2603–2610.
10 D. J. Mooney, D. F. Baldwin, N. P. Suh, J. P. Vacanti and R. Langer, *Biomaterials*, 1996, **17**, 1417–1422.
11 K. Poole, K. Khairy, J. Friedrichs, C. Franz, D. A. Cisneros, J. Howard and D. Mueller, *J. Mol. Biol.*, 2005, **349**, 380–386.
12 J. C. Schense, J. Bloch, P. Aebischer and J. A. Hubbell, *Nat. Biotechnol.*, 2000, **18**, 415–419.
13 C. A. W. Andrew, K. F. Y. Evelyn, I. C. Liao, V. Catherine Le and W. L. Kam, *J. Biomed. Mater. Res.*, 2004, **71a**, 586–595.
14 M. M. Stevens, H. F. Qanadilo, R. Langer and V. Prasad Shastri, *Biomaterials*, 2004, **25**, 887–894.
15 G. A. Silva, C. Czeisler, K. L. Niece, E. Beniash, D. A. Harrington, J. A. Kessler and S. I. Stupp, *Science*, 2004, **303**, 1352–1355.
16 X. Zhao and S. Zhang, *Trends Biotechnol.*, 2004, **22**, 470–476.
17 A. Y. Wang, X. Mo, C. S. Chen and S. M. Yu, *J. Am. Chem. Soc.*, 2005, **127**, 4130–4131.
18 J. Guan, K. L. Fujimoto, M. S. Sacks and W. R. Wagner, *Biomaterials*, 2005, **26**, 3961–3971.
19 J. Rong, L. A. Lee, K. Li, B. Harp, C. M. Mello, Z. Niu and Q. Wang, *Chem. Commun.*, 2008, 5185–5187.
20 A. Merzlyak, S. Indrakanti and S.-W. Lee, *Nano Lett.*, 2009, **9**, 846–852.
21 A. B. Michael, K. Gagandeep, L. A. Lee, X. Fang, S. Jennifer, B. Rebecca, Z. Xiongfei, J. Maisie, P. R. Thomas, E. Todd and W. Qian, *ChemBioChem*, 2008, **9**, 519–523.
22 M. Young, W. Debbie, M. Uchida and T. Douglas, *Annu. Rev. Phytopathol.*, 2008, **46**, 361–384.
23 S.-W. Lee, C. Mao, C. E. Flynn and A. M. Belcher, *Science*, 2002, **296**, 892–895.
24 P. J. Yoo, K. T. Nam, J. Qi, S.-K. Lee, J. Park, A. M. Belcher and P. T. Hammond, *Nat. Mater.*, 2006, **5**, 234–240.
25 A. Merzlyak and S.-W. Lee, *Bioconjugate Chem.*, 2009, **20**, 2300–2310.
26 J. Sambrook and D. Russell, *Molecular clonning: A Laboratory Manual*, CSHL Press, third edition, 2001.
27 H. Hatakeyama, A. Kikuchi, M. Yamato and T. Okano, *Biomaterials*, 2007, **28**, 3632–3643.
28 A. Curtis and C. Wilkinson, *Biomaterials*, 1997, **18**, 1573–1583.
29 S.-W. Lee and A. M. Belcher, *Nano Lett.*, 2004, **4**, 387–390.
30 C. Y. Chiang, C. M. Mello, J. Gu, E. C. C. M. Silva, K. J. V. Vliet and A. M. Belcher, *Adv. Mater.*, 2007, **19**, 826–832.
31 R. M. Capito, H. S. Azevedo, Y. S. Velichko, A. Mata and S. I. Stupp, *Science*, 2008, **319**, 1812–1816.
32 K. Y. Lee and D. J. Mooney, *Chem. Rev.*, 2001, **101**, 1869–1880.
33 G. W. Rebecca, *Hepatology*, 2008, **47**, 1394–1400.
34 Y. Tony, C. G. Penelope, A. F. Lisa, M. Beatrice, O. Miguelina, F. Makoto, Z. Nastaran, M. Wenyu, W. Valerie and A. J. Paul, *Cell Motil. Cytoskeleton*, 2005, **60**, 24–34.